Available online at www.sciencedirect.com
ScienceDirect
Journal of Sound and Vibration 314 (2008) 738–756
JOURNAL OF SOUND AND VIBRATION
www.elsevier.com/locate/jsvi

Sound generation in centrifugal compressors

Till Raitor*,[1], Wolfgang Neise[2]

Deutsches Zentrum für Luft- und Raumfahrt e.V. (DLR), Institut für Antriebstechnik, Abteilung Triebwerksakustik, 10623 Berlin, Germany

Received 16 January 2007; received in revised form 8 October 2007; accepted 15 January 2008
Handling Editor: C. Morfey
Available online 4 March 2008

Abstract

An experimental study is described to explore the dominant sound generation mechanisms of the spectral components governing the overall noise level of centrifugal compressors. At the design speed with supersonic flow conditions in the rotor blade channels, blade tone noise and buzz-saw noise are the main contributors. On the inlet, rotor-alone noise is the main source while rotor–stator interaction noise dominates on the outlet side in case of vaned outlet diffusers. Over a large range of rotor speeds with subsonic flow conditions, radial compressor noise is dominated by tip clearance noise which is produced by the secondary flow through the gap between rotor blade tips and the casing wall which in turn gives rise to the rotating instability phenomena observed earlier in axial-flow machines.

1. Introduction

Centrifugal compressors are used for turbocharging the diesel engines of large ships or power stations. The ever-growing demand for higher engine power output requires that mass flow rate and pressure ratio of the compressors are increased as well. While the aerodynamic power of turbomachines is proportional to the third power of the rotor tip speed, the sound power usually grows with the 5–6th power. The tonal components of the compressor noise, the so-called blade tone spectrum (blade passing frequency (BPF) and harmonics) are particularly annoying and therefore deserve special attention when it comes to reducing the noise of these machines. Primary noise reduction, i.e., noise reduction at the source, is the most efficient way to achieve quieter machines. The long-term goal of this experimental study is to reduce the blade tone noise of high-speed high-pressure centrifugal compressors. To develop primary noise reduction methods that diminish the strength of the aeroacoustic sources directly, the dominant noise generation mechanisms of centrifugal compressors have to first be known and understood.

Much research on understanding the sound generation mechanisms of turbomachines has been performed in the past, however, almost only on the axial-flow type because of its aeronautical use and public demand for

*Corresponding author.
E-mail address: till.raitor@dlr.de (T. Raitor).
[1]Dipl.-Ing., DLR, Müller-Breslau-Str. 8, 10623 Berlin, Germany.
[2]Prof. Dr. -Ing., DLR, Müller-Breslau-Str. 8, 10623 Berlin, Germany.

0022-460X/$ - see front matter
doi:10.1016/j.jsv.2008.01.034

Nomenclature

a_0	speed of sound
A	cross-sectional area ($A_0 = 1\,\mathrm{m}^2$)
c	blade chord length
d	duct diameter
f	frequency
f_{BPF}	blade passage frequency ($= Zf_n$)
$f_{c(m,n)}$	cut-on frequency of the mode (m,n)
f_n	rotor shaft frequency
h	harmonic of blade passage frequency
h_α	harmonic of RI component
i	harmonic of rotor shaft frequency
L_p	pressure level at $p_0 = 20\,\mu\mathrm{Pa}$
L_W	sound power level at $P_0 = 1\,\mathrm{pW}$
m	azimuthal mode order
$\dot{m}, \dot{m}_{\mathrm{red}}$	mass flow, reduced mass flow
Ma	tip speed Mach number
n	radial mode order
n, n_{red}	rotor speed, reduced rotor speed
p	pressure
P	power
T	absolute temperature
U	rotor tip speed
Z	number of main rotor blades
α_{RI}	azimuthal mode order of RI component
Π_{tot}	total pressure ratio
ρ	density
ω	angular frequency
Ω	angular velocity
BPF	blade passage frequency
id	inlet duct
iid	immediate inlet duct
od	outlet duct
R	rotor
RI	rotating instability
TCN	tip clearance noise

quieter aircraft. Experimental or theoretical studies on the radial flow type were limited to the low-speed machines as used in air conditioning and ventilating industries. The first experimental study on centrifugal compressor noise addressing the sound field radiated into the inlet and outlet ducts was published by Feld et al. [1] when the present investigation had just been started.

In the present research project, detailed acoustic measurements are carried out on two shroudless radial impellers type SRV2 (with a vaneless and a vaned outlet diffuser) and type SRV4 (with vaneless outlet diffuser) running on a typical compressor test bed. To the authors' knowledge, the research project is the first systematic investigation of the dominant sound generation mechanisms in radial compressors.

Sound power measurements at various operating lines of the compressors are made in the anechoically terminated inlet duct following a standardized measurement procedure to establish a database for the acoustic sound power of centrifugal compressors. Based on the measurement data, an empirical model for the sound power of radial compressors as function of the main dimensions and the operational parameters is developed which will be the subject of a subsequent paper.

Acoustic mode measurements are made in the inlet duct at two different axial positions with different diameters: immediately upstream of the compressor intake and 2.1 m farther upstream using rotatable duct sections. Both are equipped with four axial rings with four wall-flush mounted condenser microphones each. The microphones are traversed circumferentially to resolve the spatial sound pressure distribution into azimuthal duct modes of the blade tones up to 40 kHz. The modal structure of the sound radiated from the compressor impeller reveals the dominant sound generation mechanisms at various speed ranges. The relative importance of the different source mechanisms depending on rotor speed is described.

Measurements of the unsteady wall pressure along the radial extent of the compressor casing provide insight into the flow processes within the rotating rotor blade channels and allow comparisons with previous CFD analyses. In particular, the rotor-coherent pressure field at the impeller intake was computed using the DLR code TRACE. Steady flow conditions were assumed in the rotating impeller channels. The results were converted to an unsteady pressure field at the impeller intake and compared with acoustic measurement data.

In the present paper, emphasis is placed on describing the generation mechanisms of the spectral components governing the overall noise level of centrifugal compressors. For more detailed information and other findings, see Refs. [2–5].

2. Experimental facility

2.1. Test rig

The experiments were made in the radial compressor test facility of the DLR-Institute of Propulsion Technology in Cologne (see the principal sketch depicted in Fig. 1). This rig was specifically designed for transonic flow investigations and analyses [6–11] and was modified for the acoustic measurements described here.

On the intake side of the compressor, there is a filter section, a Venturi tube for measurement of the mass flow, an anechoic duct termination to prevent the sound radiated from the compressor to be reflected at duct discontinuities, the acoustic duct section, and a bellmouth nozzle connecting the 500 mm diameter acoustic duct to the 157 mm diameter inlet pipe mounted at the compressor intake.

In the acoustic test duct, a $\frac{1}{2}$-in microphone equipped with a special turbulence screen is mounted in a rotatable duct section (see Fig. 2) to measure the circumferentially averaged sound pressure level at a specified radial distance from the duct axis as required by the standardized measurement procedure ISO 5136 [12] for determination of the in-duct sound power radiated by the compressor into the inlet duct. For acoustic mode analyses, the rotatable duct can also be instrumented with condenser microphones mounted flush with the inner duct wall and arranged in four axial rings with four microphones each.

Another rotatable duct section is available in the 157 mm diameter inlet pipe. Again, 4×4 wall-flush mounted condenser microphones are used to measure the acoustic pressures at the inner duct wall and resolve its spatial distribution into acoustic duct modes. At this measurement station, the temporal and spatial sound field structures generated by the compressor exist without any changes due to duct transmission effects, which is important in view of the identification of the main sound generation mechanisms prevalent in this type of turbomachine.

Up to eight piezoresistive differential pressure sensors can be mounted in the casing wall to monitor the rotating pressure field of the shroudless impeller. Five of these positions were used for the present experiments. Position no. 1 is located at the leading edge of the main rotor blades, position no. 2 at the leading edge of the splitter blades, position no. 3 at the last one-third of the rotor blade channel, position no. 4 at the blade trailing edges, and position no. 5 at the radial location of the leading edge of the exit guide vanes, if present. Ideally, one would want to place the transducers in the casing along the curve of a rotor blade. This is not possible for space reasons and therefore the transducers at the various radial positions are displaced circumferentially by one or more full blade pitches.

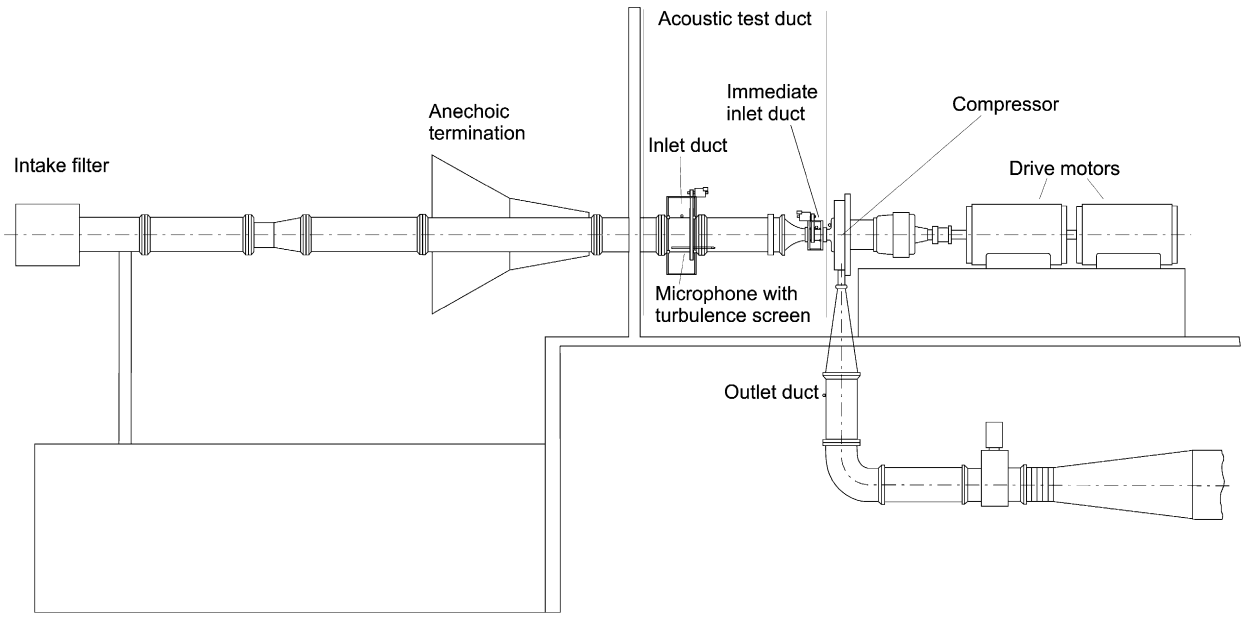

Fig. 1. Schematic view of the DLR radial compressor test facility.

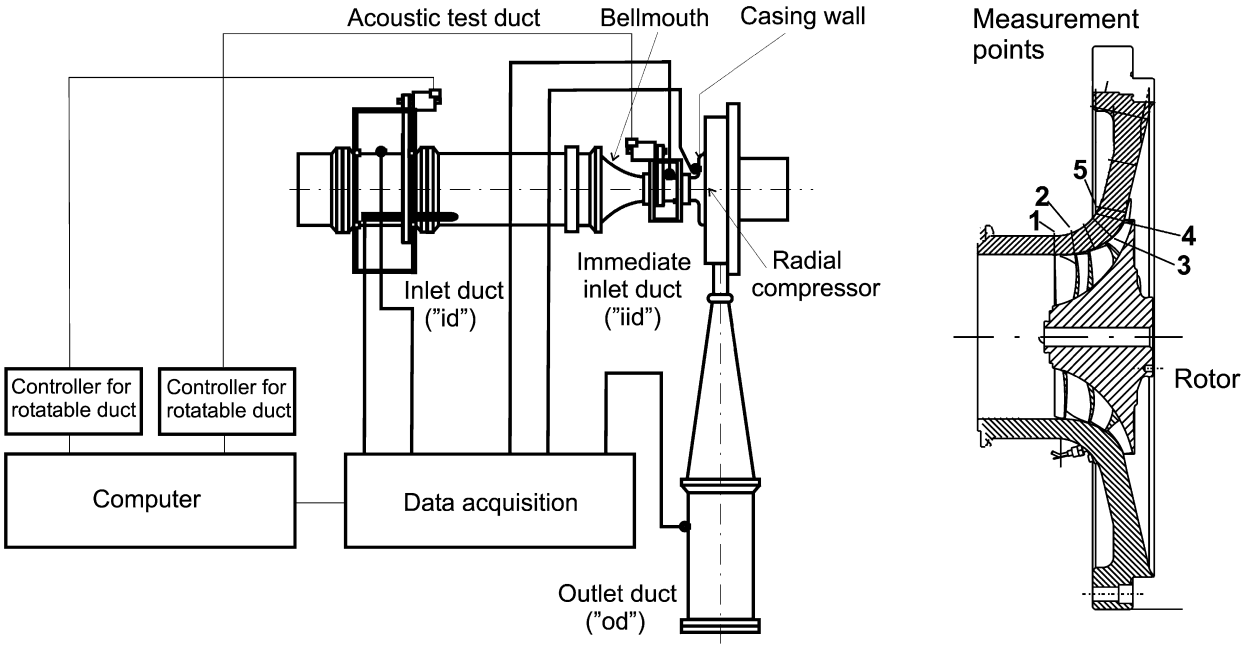

Fig. 2. Acoustic measurement positions in the compressor inlet and outlet duct and on the casing of the shroudless compressor.

The compressor outlet ducting is far from ideal for acoustic measurements. There is only a very short straight duct section between an outlet flow diffuser and a 90° duct bend. Up to five wall-flush pressure sensors can be mounted in the 309 mm diameter duct section to monitor the sound pressure spectrum radiated into the outlet duct. It is not possible to determine the radiated sound power from the measured sound pressure, nor is it meaningful to perform acoustic mode analyses for investigation of sound generating mechanisms.

2.2. Test compressors

Measurements were made with two impellers type SRV2 and type SRV4, the first in a vaneless and a vaned diffuser configuration and the latter in a vaneless configuration only. Both impellers have 156 mm leading edge tip diameter, 224 mm outer impeller tip diameter, 13 main rotor blades and 13 splitter blades. Fig. 3 shows the performance characteristics of the test compressors SRV2 and SRV4, both with vaneless diffuser, and the operating conditions for the acoustic measurements. The following aerodynamic flow parameters are used to characterize the performance of the test compressors as functions of rotor speed n, mass flow $\dot{m}$, absolute temperature T and pressure p:

$$n_{\mathrm{red}} = n\sqrt{T_{00}/T}, \quad \dot{m}_{\mathrm{red}} = \dot{m}\sqrt{(T/T_{00})}\,(p_{00}/p), \tag{1}$$

where $T_{00} = 288.15\,\mathrm{K}$ and $p_{00} = 101.325\,\mathrm{kPa}$.

For the compressor SRV2 (design point $\dot{m}_{\mathrm{red}} = 2.55\,\mathrm{kg/s}$ at $n_{\mathrm{red}} = 50{,}000/\mathrm{min}$) measurements were made at

- constant rotor speed $n_{\mathrm{red}} = 50{,}000/\mathrm{min}$ and variable throttle condition in the range $\dot{m}_{\mathrm{red}} = 2.3 - 2.8\,\mathrm{kg/s}$,
- constant throttle and variable rotor speed in the range $n_{\mathrm{red}} = 30{,}000$–$50{,}000/\mathrm{min}$ and
- constant pressure ratio $\Pi_{\mathrm{tot}} = 4.0$ in the range $\dot{m}_{\mathrm{red}} = 1.8 - 2.8\,\mathrm{kg/s}$.

For the compressor SRV4 (design point $\dot{m}_{\mathrm{red}} = 2.55\,\mathrm{kg/s}$ at $n_{\mathrm{red}} = 50{,}000/\mathrm{min}$) measurements were made at

- constant rotor speed $n_{\mathrm{red}} = 50{,}000/\mathrm{min}$ and variable throttle condition in the range $\dot{m}_{\mathrm{red}} = 2.3 - 2.8\,\mathrm{kg/s}$,
- constant rotor speed $n_{\mathrm{red}} = 36{,}000/\mathrm{min}$ and variable throttle condition in the range $\dot{m}_{\mathrm{red}} = 1.1 - 2.1\,\mathrm{kg/s}$,

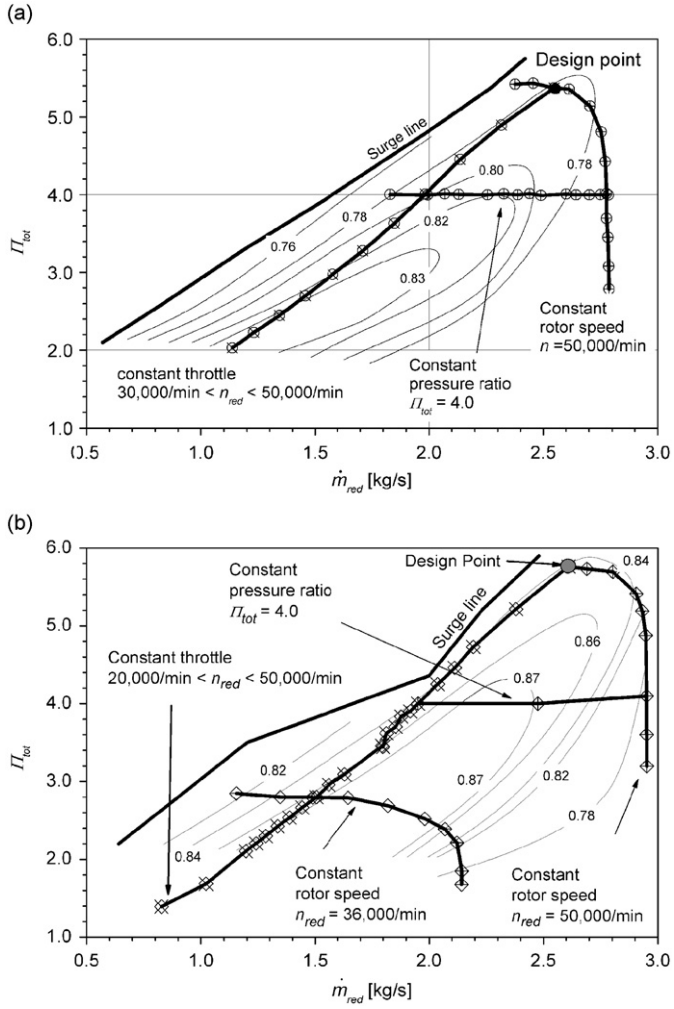

Fig. 3. Compressor characteristics and operating conditions for the acoustic measurements: (a) SRV2 with vaneless diffuser and (b) SRV4 with vaneless diffuser.

- constant throttle and variable rotor speed in the range $n_{\mathrm{red}} = 20{,}000$–$50{,}000$/min, and
- constant pressure ratio $\Pi_{\mathrm{tot}} = 4.0$ in the range $\dot{m}_{\mathrm{red}} = 1.8 - 2.8\,\mathrm{kg/s}$.

3. Experimental results

3.1. Spectral characteristics of radial compressor noise

In Fig. 4 are plotted the sound pressure spectra measured at the interior wall of the immediate inlet duct of the compressor SRV2 without outlet guide vanes at constant throttle in the speed range 30,000–50,000/min. At each speed, the BPF component is clearly visible in the spectrum. In this paper, the BPF is defined as the product of the rotor shaft frequency f_n and the number of main rotor blades Z, i.e., $f_{\mathrm{BPF}} = Zf_n$.

With increasing harmonic order h, the levels of the blade tone harmonics hf_{BPF} become smaller. The higher the rotor speed, the more prominent are the BPF and its harmonics the BPF and its harmonics.

Above 40,000/min, the rotor shaft speed harmonics if_n become important until finally at 50,000/min the harmonics $i = 6$ and 7 reach levels almost as high as that of the BPF. Aero-engines operating with supersonic fan tip speeds are known to generate a tonal sound spectrum spread over a range of harmonics of the engine

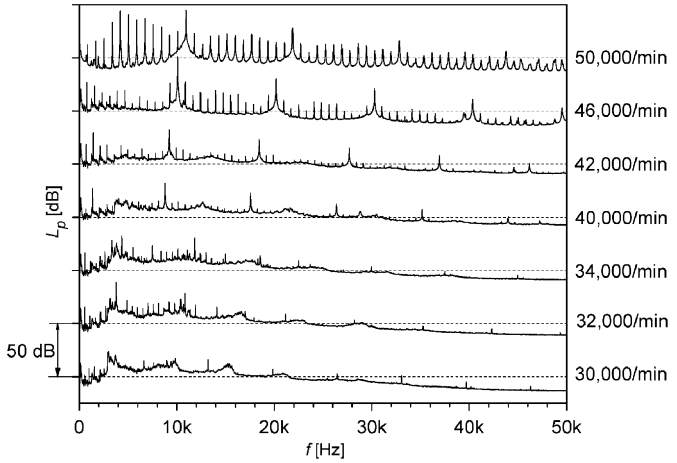

Fig. 4. Circumferentially averaged sound pressure spectra in the compressor immediate inlet duct as function of the rotor speed; SRV2, vaneless diffuser (for clarity, individual spectra are shifted vertically by 50 dB).

shaft rotation frequency. These harmonics are commonly termed "buzz-saw" tones. The pressure signature attached to a supersonic ducted fan will be a saw tooth waveform. These rotor-speed harmonics are caused by the shock waves in the rotating blade channels, which in the present case begin to exist at a rotor speed of 41,000/min.

At the low rotor speeds 30,000–34,000/min, narrow-band noise components are observed at about half the BPF, which increase with speed. At 30,000 and 32,000/min, the levels of the narrow-band components are higher than the BPF level and therefore dominate the overall noise of the compressor.

It will be shown later in this paper (Section 3.3.4) that the narrow-band components are produced by the secondary flow through the gap between the compressor casing and the impeller blade tips, similar to the "tip clearance noise" (TCN) observed in axial-flow machines by Kameier [13] and Kameier and Neise [14]. Further experimental and numerical investigation of the rotating instability (RI) mechanisms were presented by März et al. [15]. For brevity, the expression "TCN" will be used in the following to refer to the narrow-band spectral components below the BPF even though the experimental proof for that is yet to be presented.

In Fig. 5a–c, the sound pressure spectra measured at the interior duct wall of the immediate inlet duct are plotted for all compressor configurations tested. On the left-hand side spectra are presented as contour plots, and on the right-hand side the same data are given in a three-dimensional plot. The change in spectral characteristics with rotor speed is similar for all the three compressor configurations. TCN has the highest levels at low speeds; it disappears from the spectrum above 40,000/min in case of the SRV2 (Fig. 5a and b), but prevails up to 46,000/min in case of SRV4 (Fig. 5c). Comparing Fig. 5a and b shows that the TCN is somewhat diminished by the presence of the vaned diffuser.

3.2. Sound fields in the inlet and outlet duct

3.2.1. Sound pressure spectra in the inlet duct

Sound pressure spectra measured at the design point of SRV2 ($n_{\mathrm{red}} = 50{,}000/\mathrm{min}$, $\dot{m}_{\mathrm{red}} = 2.55\,\mathrm{kg/s}$) in the immediate inlet duct and the inlet duct are plotted in Fig. 6a. The BPF-component has the highest level, and its harmonics (hf_{BPF}) are always higher in level than the neighbouring spectral components. In addition to the blade tone spectrum, the rotor shaft speed harmonics (buzz-saw noise) are also clearly visible. At this high rotor speed, the presence of the outlet guide vanes has very little effect on the sound spectra measured on the compressor inlet side because any noise components generated by rotor–stator interaction could not propagate upstream through the transonic flow fields in the rotor blade channels.

The spectral content of the sound spectra changes when propagating upstream from the rotor inlet plane into the immediate inlet duct ($d_{\mathrm{iid}} = 157\,\mathrm{mm}$) and further into the inlet duct ($d_{\mathrm{id}} = 500\,\mathrm{mm}$) which is due to the sound transmission and reflection characteristics of the ducts and the bellmouth nozzle and by nonlinear

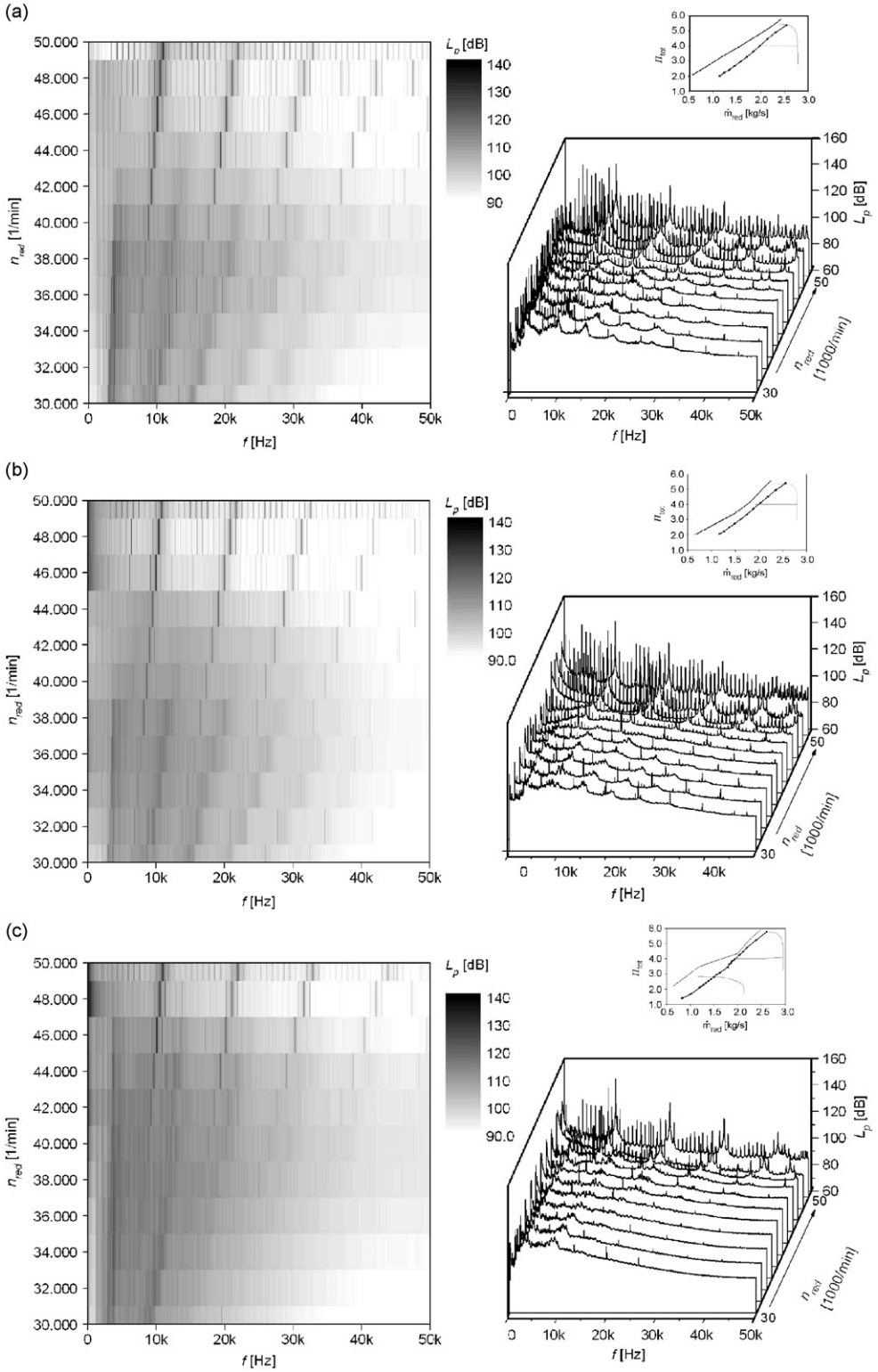

Fig. 5. Spectral characteristics of radial compressor noise as function of rotor speed: (a) SRV2, vaneless diffuser, (b) SRV2, vaned diffuser and (c) SRV4, vaneless diffuser (operating line "constant throttle", compare Fig. 3).

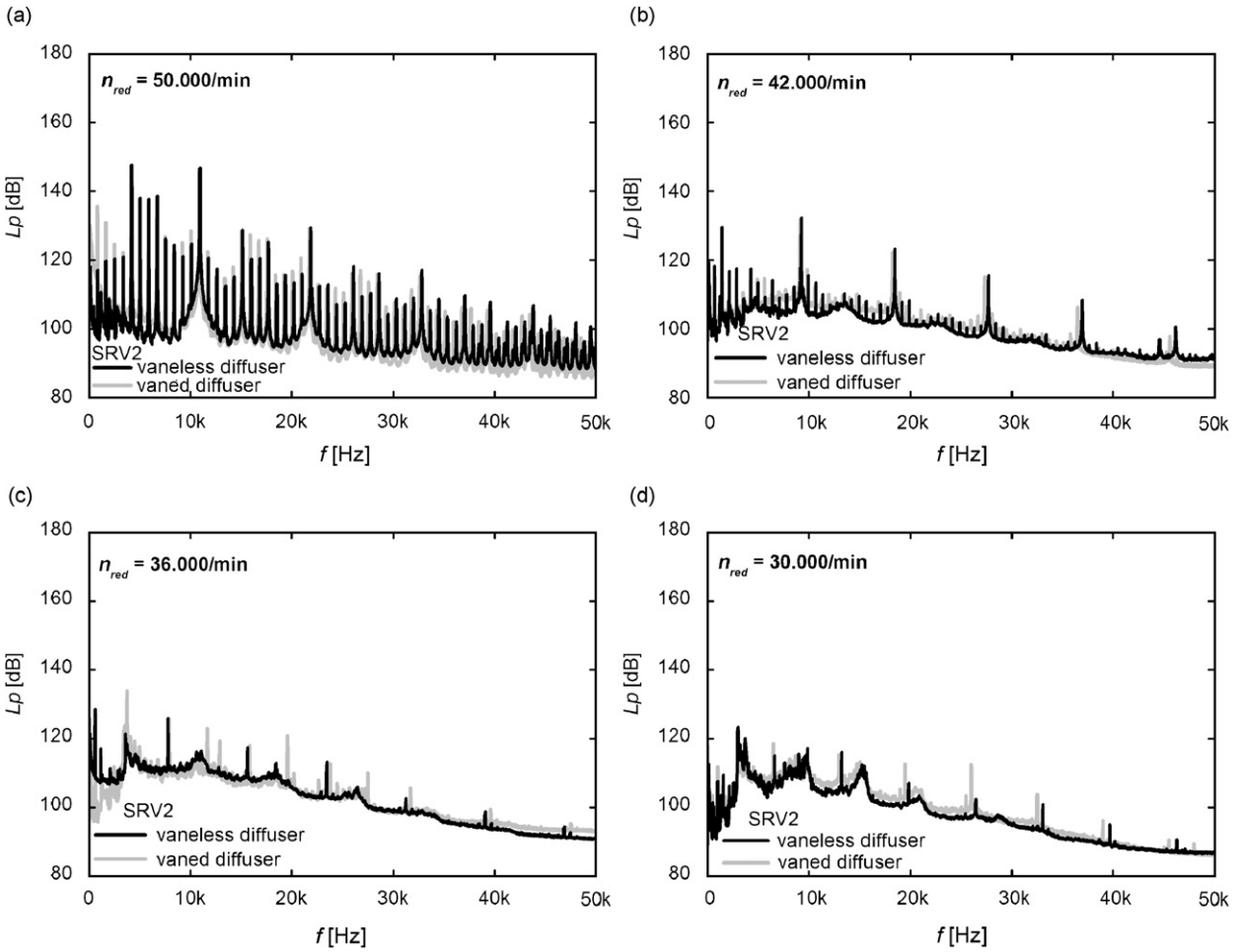

Fig. 6. Sound pressure spectra in the immediate inlet duct; SRV2 (operating line "constant throttle").

damping effects which particularly affect low-frequency components composed from evanescent acoustic duct modes.

To illustrate the damping effect, the levels of the first 14 rotor-speed harmonics ($i = 1$–14) are plotted in Fig. 7 for the wall pressure on the compressor casing (measurement point #1, compare Fig. 2) and the sound pressure in the immediate inlet duct. The axial distance between the two measurement stations is 289 mm, i.e., $1.84 d_{\mathrm{lid}}$.

At the casing wall, the BPF level is 25 dB higher than those of the next higher rotor-speed harmonics ($i = 5$ and 14), and except for $i = 2$ the levels of the rotor-speed harmonics are distributed fairly evenly. While propagating from the rotor inlet plane (MP#1) to the acoustic measurement station in the immediate inlet duct, the various rotor-speed harmonics are damped to different degrees.

Each rotor-speed harmonic i of buzz-saw noise is formed by only one azimuthal mode with its mode order being equal to the rotor-speed harmonic order: $m = i$ (see e.g., McAlpine et al. [16]). In the case considered in Fig. 7, the modes $m = 1$–4 are not propagational in the immediate inlet duct at their respective frequencies and are therefore substantially reduced in level. Conversely, the mode $m = 5$ of the rotor-speed harmonics $i = 5$ at $5 f_n = 4193$ Hz is excited just above its cut-on frequency and propagates down the duct with little change in level. Similarly, for the harmonics $i = 6$–8.

Fig. 6a–d shows the change of the sound pressure spectra in the immediate inlet duct when the compressor speed is changed from 50,000/min down to 30,000/min in a little more detail. At $n_{\mathrm{red}} = 50{,}000$ and 42,000/min, the overall sound pressure level is dominated by the BPF component while at $n_{\mathrm{red}} = 36{,}000$ and 30,000/min a

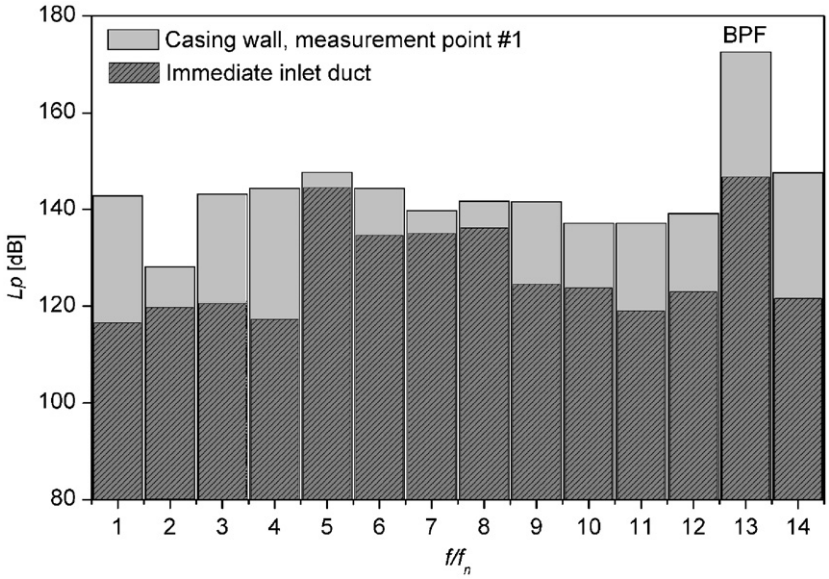

Fig. 7. Comparison of rotor-speed harmonic levels at the casing wall (MP#1, compare Fig. 2) and in the immediate inlet duct; SRV2; vaneless diffuser; $n_{red} = 50{,}000$/min; operating line "constant throttle".

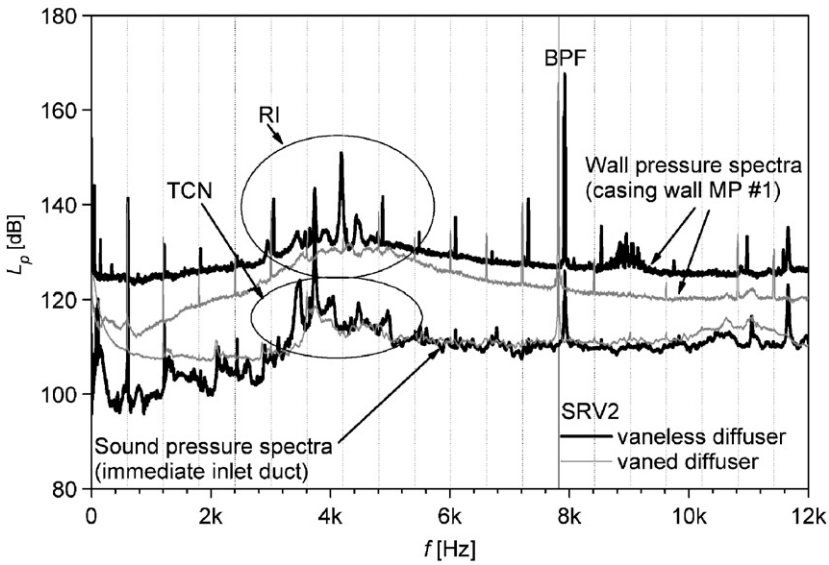

Fig. 8. Comparison of sound pressure spectra in the immediate inlet duct and wall pressure spectra at the compressor casing wall (MP#1); SRV2, $n_{red} = 36{,}000$/min (operating line "constant throttle").

narrow-band component at about half the BPF exhibits maximum levels. Other relative level maxima are observed at $1.5f_{BPF}$.

In Fig. 8, the sound pressure spectra from Fig. 6c for 36,000/min are shown in an expanded frequency scale together with the wall pressure spectra measured on the casing wall (MP#1, see Fig. 2). The frequency range of TCN is marked in the sound pressure for the immediate inlet duct. A similar hump appears in the wall pressure spectra between 2.8 and 5.0 kHz, which is termed "RI". This phenomenon was first observed by Kameier [13] on a high-pressure axial-flow fan and found to be the cause of the TCN. This noise generation mechanism will be discussed further in Section 3.3.4.

3.2.2. Comparison of sound pressure spectra in the inlet and outlet duct

In Fig. 9, sound pressure spectra in the immediate inlet duct and outlet duct are compared for SRV2 with outlet guide vanes. To account for the different cross-sectional areas ($d_{iid} = 157$ mm; $d_{od} = 309$ mm), the outlet duct spectra were raised by an increment

$$K_A = 20\,lg(d_{od}/d_{iid}) = 5.9\,\text{dB}. \tag{2}$$

At the design point ($n_{red} = 50{,}000$/min), the inlet duct sound pressure spectrum is dominated by the BPF and buzz-saw noise components, as was observed before. In the outlet duct, rotor-speed harmonics are found only below the BPF with levels substantially lower than on the inlet side. Obviously, shock fronts attached to the rotor blades radiate sound efficiently in the upstream but not in the downstream direction. The outlet duct random noise levels are higher than the ones in the inlet duct up to 28 kHz.

At $n_{red} = 42{,}000$/min, the tonal noise components in the outlet duct are higher in level than on the inlet side. This clearly demonstrates that the rotor–stator interaction is important for the noise radiation into the outlet duct but not for the inlet side. For example, the outlet duct BPF level is 142.1 dB compared with 129.3 dB in the immediate inlet duct. Beginning at 13 kHz, the random noise levels on the outlet side decrease more strongly with frequency than on the inlet side.

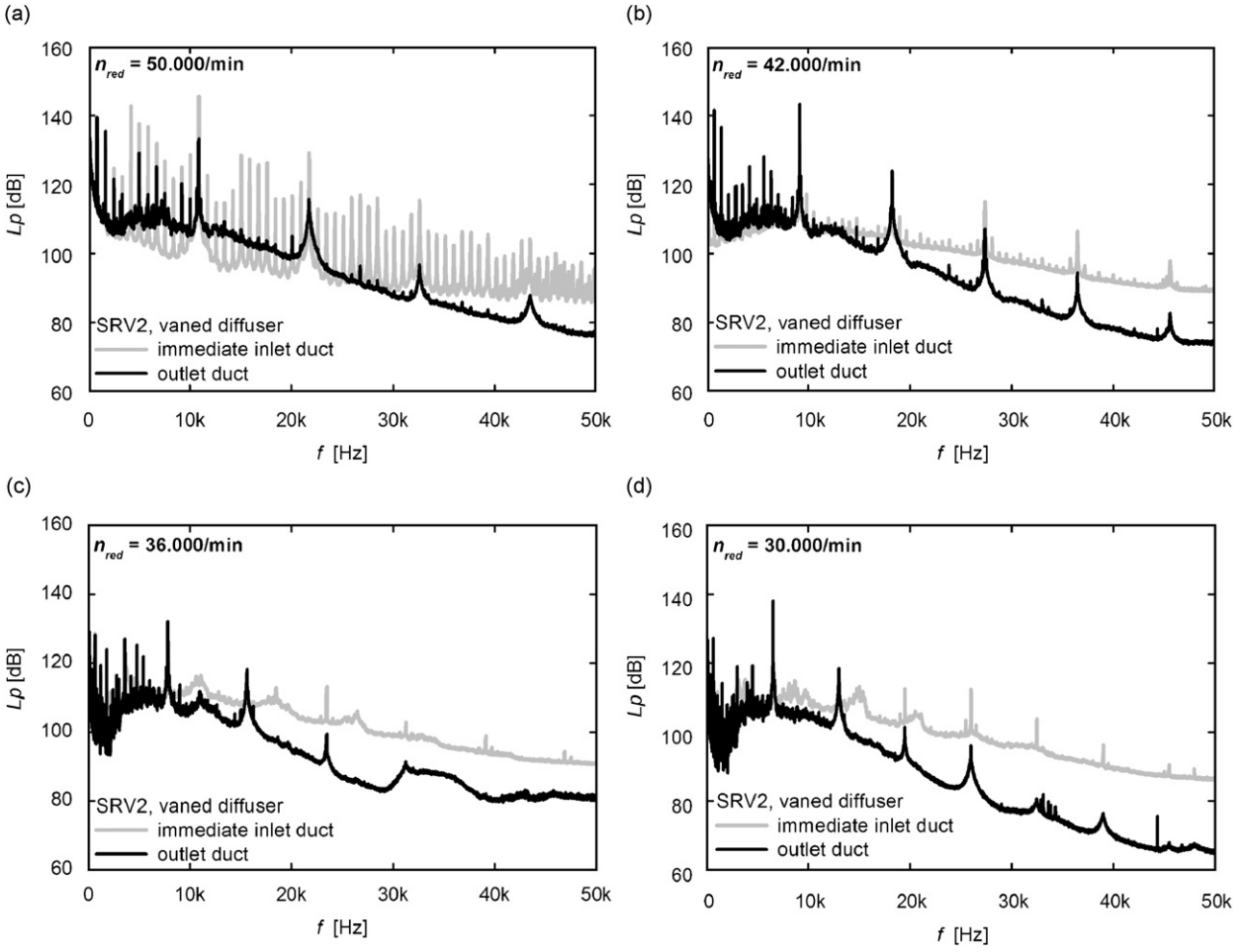

Fig. 9. Comparison of sound pressure spectra in the immediate inlet duct and outlet duct (levels raised by $K_A = 5.9$ dB); SRV2; vaned diffuser; operating line "constant throttle".

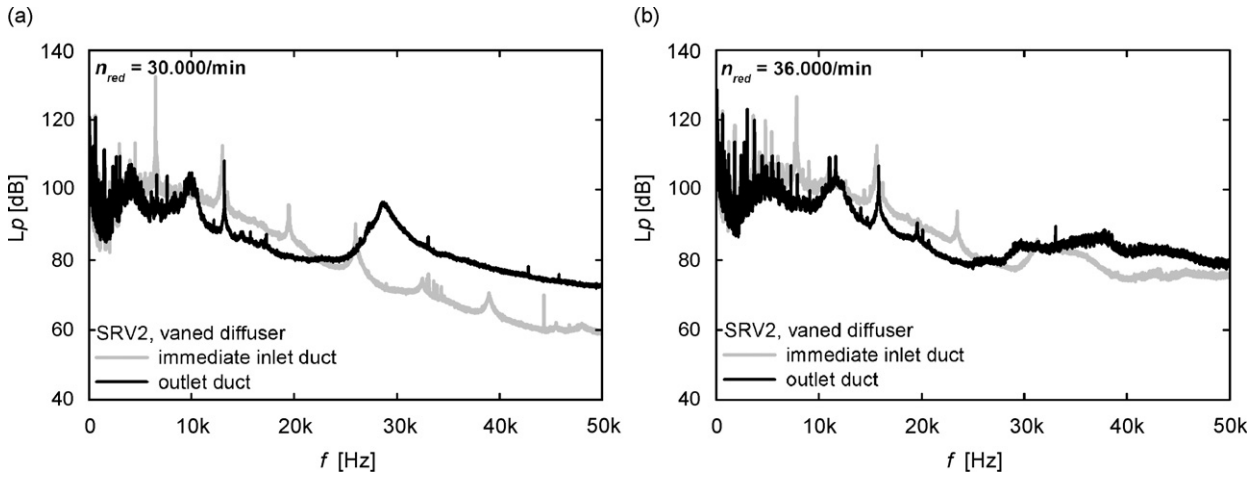

Fig. 10. Effect of the outlet guide vanes on the sound pressure spectra in the outlet duct; SRV2; operating line "constant throttle".

At the two lower speeds 30,000 and 36,000/min the TCN components are more pronounced on the inlet side. But note that the data in Fig. 9 are for the vaned diffuser where TCN was observed to be weaker than with the vaneless diffuser.

The effect of the outlet guide vanes on the sound pressure spectra in the outlet duct is presented in Fig. 10 for rotor speeds of 30,000 and 36,000/min. At both speeds, the BPF component dominates the overall noise level when the outlet guide vanes are in place, but not so with the vaneless diffuser. TCN is clearly visible below and above the BPF with the vaneless diffuser and much less distinct with outlet guide vanes.

3.2.3. *Overall sound pressure and sound power in the inlet duct*

In Fig. 11 are plotted the total sound pressure level $L_{p,\mathrm{tot}}$ (0–50 kHz) and the BPF level $L_{p,\mathrm{BPF}}$ in the immediate inlet duct (top diagram), the total sound pressure $L_{p,\mathrm{tot}}$ (0–50 kHz) and the BPF level $L_{p,\mathrm{BPF}}$ in the inlet duct (middle diagram), and the total sound power level $L_{W,\mathrm{tot}}$ (50 Hz–20 kHz) and BPF one-third octave band power level $L_{W,\mathrm{BPF}}$ (bottom diagram) as functions of the reduced rotor speed at constant throttle. The sound power in the inlet duct was determined based on the standardized in-duct measurement procedure ISO 5136 [12] in one-third octave bands.

The total sound power level L_W increases with the rotor speed up to $n_{\mathrm{red}} = 36{,}000$/min where a relative maximum is reached. Above 36,000/min there is a slight decrease of $L_{W,\mathrm{tot}}$ and a subsequent rise beginning at 44,000/min. These general trends can be observed a little more clearly in overall sound pressure levels $L_{p,\mathrm{tot}}$ in the immediate inlet duct and the inlet duct (top and middle diagram of Fig. 11).

In the speed range up to 36,000/min, TCN is the strongest spectral component and dominates the overall noise level. At higher speeds, TCN becomes weaker, and the blade tone levels grow. At 41,000/min the flow at the blade tip at the rotor inlet plane becomes supersonic, however, without a significant change in the noise. A noticeable noise level increase does not occur until rotor speeds between 44,000 and 46,000/min. The reason for this behaviour is that the BPF component, as will be shown in Section 3.3.2, is dominated by a single azimuthal duct mode $m = 13$ which is cut off below 45,000/min and contributes to the far-field sound level only above this rotor speed, compare the BPF-level distribution in the top diagram of Fig. 11.

The exact reason for the speed dependence of the TCN is not known. A possible explanation is that the radial tip clearance gap varied with rotor speed due to blade deflections under centrifugal and/or thermal stresses and/or due to the speed characteristics of the rotor shaft bearing system. During the experiments the tip clearance gap was monitored only at the impeller exit to avoid rubbing contact of impeller and casing but not at the impeller inlet plane or intermediate stations. Another possible explanation lies of course in the aerodynamics of the blade tip flow, which certainly change when the flow conditions become sonic. It

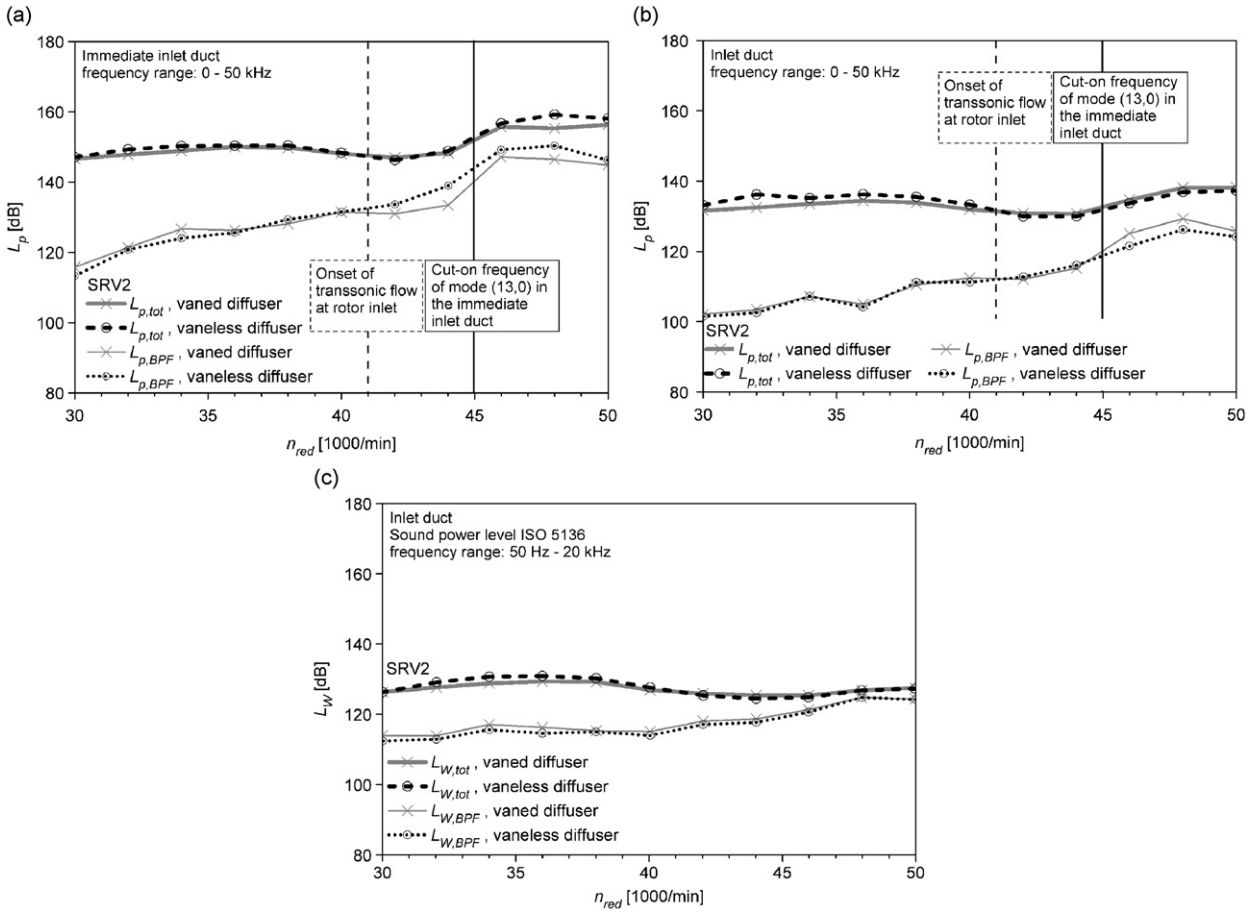

Fig. 11. Radial compressor noise levels in the inlet duct versus reduced rotor speed; SRV2; operating line "constant throttle": (a) sound pressure level in the immediate inlet duct, (b) sound pressure level in the inlet duct and (c) sound power level in the inlet duct.

was observed before in Fig. 5 that TCN is present up to 40,000/min in case of the impeller SRV2 and up to 46,000/min in case of SRV4, for the same nominal tip clearance gap, which is an indication that the impeller design and aerodynamics may have an effect on this phenomenon. However, since neither detailed tip clearance measurements nor tip clearance flow measurements were performed in the speed range in question, the reason for the speed dependence of the TCN remains unclear.

The influence of the outlet guide vanes on the overall sound power is not very pronounced. Up to 41,000/min, $L_{W,\mathrm{tot}}$ is by about 2 dB higher with the vaneless diffuser, which is due to the weaker TCN in this case.

3.2.4. Overall sound pressure in the outlet duct

The overall sound pressure levels in the outlet duct of the SRV2 compressor are depicted in Fig. 12 as functions of the reduced rotor speed for the cases without and with outlet guide vanes. The corresponding levels in the compressor immediate inlet duct are repeated from Fig. 11a for direct comparison. The effect of the vaned diffuser is to increase the overall outlet level by about 3.5 dB on average, which is of course due to the rotor–stator interaction that generates tonal components in the outlet duct. This result is in accordance with investigations by Feld et al. [1].

In the lower rotor-speed range up to 40,000/min, the inlet and outlet levels obtained with the vaned diffuser differ by only 0.7 dB, on average. However, with the vaneless diffuser, the average difference between inlet and outlet sound pressure levels is as large as 6 dB in the same speed range.

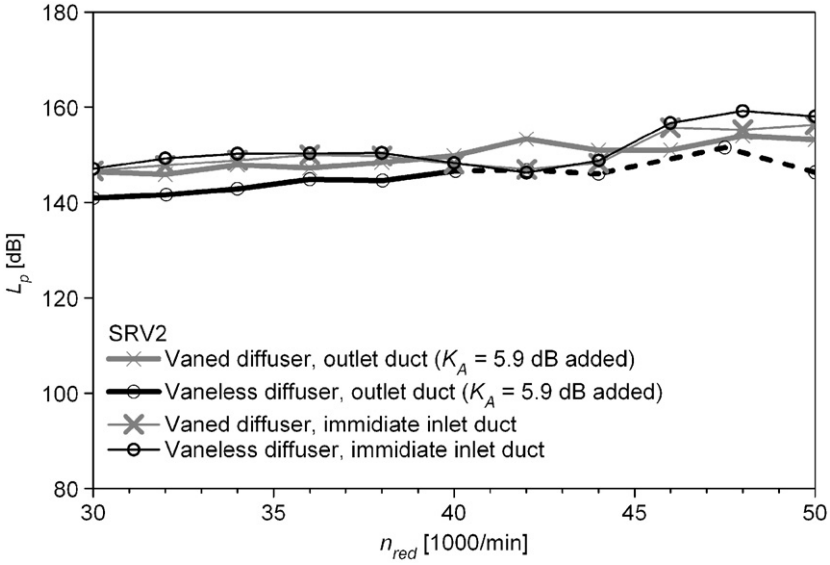

Fig. 12. Comparison of inlet and outlet duct total sound pressure levels ($K_A = 5.9$ dB increment added to outlet levels); SRV2; operating line "constant throttle".

While the inlet sound pressure levels reach their relative minimum at 42,000/min, as discussed before, the outlet sound pressure level of the SRV2 with outlet guide vanes exhibits a relative maximum. In the speed range 46,000–50,000/min, the outlet duct levels are lower than those in the immediate inlet duct.

3.3. Acoustic mode analysis for source mechanism identification

3.3.1. Introductory remarks

In this section, frequency and acoustic mode analyses are described which are useful to identify and characterize the aeroacoustic generation mechanisms of various spectral components of centrifugal compressor noise. The mode analyses are carried out in the inlet duct immediately upstream of the impeller inlet plane where the spatial sound field structure generated by the turbomachine exists without secondary influences of sound propagation, transmission or reflections.

In this context, it is useful to recall Tyler's and Sofrin's [17] famous relationship for the acoustic mode orders generated by rotor–stator interaction

$$m_{R\&S} = h\,Z - s\,V \tag{3}$$

in which Z and V are the number of rotor blades and stator vanes; $h = 1, 2, \ldots$ stand for the BPF and its harmonics, and $s = \ldots, -2, -1, 0, 1, 2\ldots$. If there are no vanes or other flow disturbances to interact with the rotor, i.e., $V = 0$, from Eq. (3) follows for the rotor-alone tonal noise $m_R = hZ$.

3.3.2. Blade tone components

In Fig. 13a and b are shown the azimuthal mode spectra of the BPF f_{BPF} and its first harmonic $2f_{\mathrm{BPF}}$ at the design point of SRV2 without outlet guide vanes: In both diagrams, the mode spectra in the immediate inlet duct are dominated by only one mode, i.e., $m = 13$ for f_{BPF} (23 dB over the level of second highest mode $m = 12$) and $m = 26$ for $2\,f_{\mathrm{BPF}}$ (15 dB over the level of second highest mode $m = 2$), which in the light of Eq. (3) reveals that these blade tones are generated by the pressure fields attached to the rotor blades, by rotor-alone noise, and not by any interference of the rotor with surrounding flow fields.

When the outlet guide vanes are added, the mode spectra on the compressor inlet side are dominated by the same mode orders $m = 13$ and 26, respectively (mode spectra not shown here). Hence, rotor–stator interaction does not play a role for the tonal compressor noise on the inlet side at the design speed. The reason for that

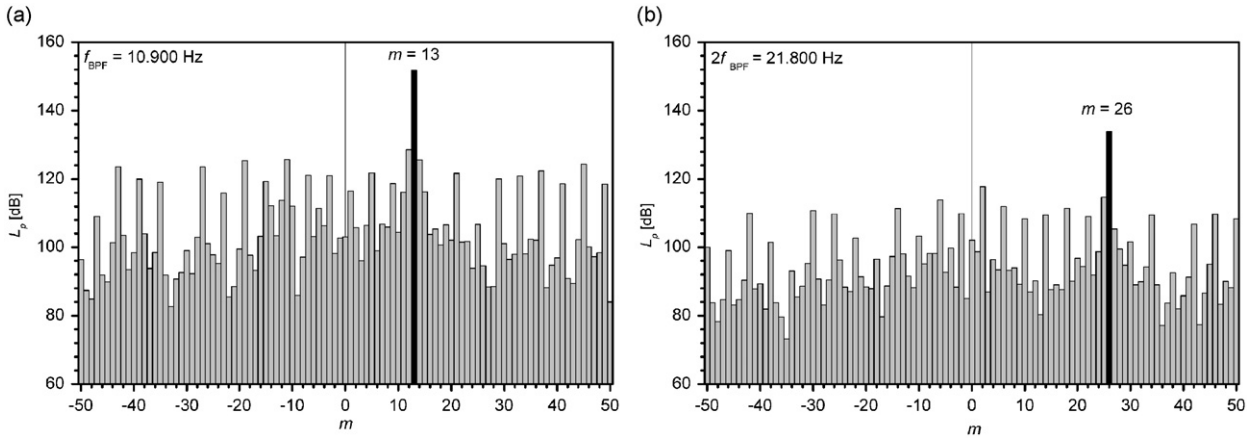

Fig. 13. Azimuthal mode spectra in the immediate inlet duct; SRV2; vaneless diffuser; design point; $n_{red} = 50{,}000$ min, $\dot{m}_{red} = 2.56\,kg/s$, $\Pi_{tot} = 5.44$: (a) $f_{BPF} = 10{,}900$ Hz and (b) $2\,f_{BPF} = 21{,}800$ Hz.

was given earlier in this paper: disturbances due to rotor–stator interaction certainly exist downstream of the rotor, but they cannot propagate through the transonic flow regimes in the rotating blade channels into the inlet duct.

The dominance of the modes $m = 13$ and 26 described above was also observed in the inlet duct of 500 mm diameter, because modes that are cut on in the immediate inlet duct are also propagational in the inlet duct of larger cross-section.

At the rotor speed $n_{red} = 42{,}000$/min (no spectrum shown here), the BPF component is $f_{BPF} = 9147$ Hz. In the immediate inlet duct, the mode $m = 13$ lies just outside the range of propagational modes at this frequency and, therefore, has a much lower level than the modes of lower order which are inside the range of cut-on modes. Since the cut-off mode $m = 13$ cannot propagate through the immediate inlet duct, it is also unimportant in the larger inlet duct although it falls in the range of cut-on modes there.

The above discussion helps to explain the dependence of the sound pressure and sound power level on the rotor speed depicted in Fig. 11. Despite the onset of transonic flow, the overall levels diminish at $n_{red} = 41{,}000$/min because the mode $m = 13$ is cut off. The subsequent increase at $n_{red} = 45{,}000$/min is due to the mode $m = 13$ at BPF cutting on which makes the BPF the dominant spectral component in the inlet duct.

3.3.3. *Buzz-saw noise components*

As mentioned before, turbomachines operating with supersonic fan tip speeds are known to generate a tonal sound spectrum spread over a range of harmonics of the engine shaft rotation frequency. These harmonics are commonly termed "buzz-saw" tones. The principal source of buzz-saw noise is the rotor-alone pressure field, which is steady in the rotor frame of reference, i.e., the pressure field locked to the rotor. At supersonic tip speeds, the rotor-locked pressure field is dominated by the shock waves attached to the blades, and the associated rotor-alone pressure field propagates upstream in the inlet duct (see Morfey and Fisher [18], Hawkings [19], Stratford and Newby [20] and Fisher et al. [21]).

The rotor-alone pressure field comprises a number of spinning modes that have the same rotational velocity as the rotor. As stated before, each of rotor-speed harmonic i of buzz-saw noise comprises only one azimuthal mode the order of which is equal to the rotor-speed harmonic order: $m = i$. The angular frequency ω_M of these modes is given by

$$\omega_M = i\,2\pi f_n. \tag{4}$$

In Fig. 14a is depicted the rotor-coherent components of the sound pressure spectrum measured in the immediate inlet duct for the impeller SRV2 with the vaneless diffuser at a rotor speed of $n_{red} = 50{,}000$/min. Owing to the phase averaging of the spectra, the random noise components of the pressure signal are suppressed, and the rotor harmonics and the BPF are more pronounced than in conventionally averaged spectra. In Fig. 14b–d, azimuthal mode spectra are shown for the rotor-speed harmonics $i = f/f_n = 4$, 5 and 6.

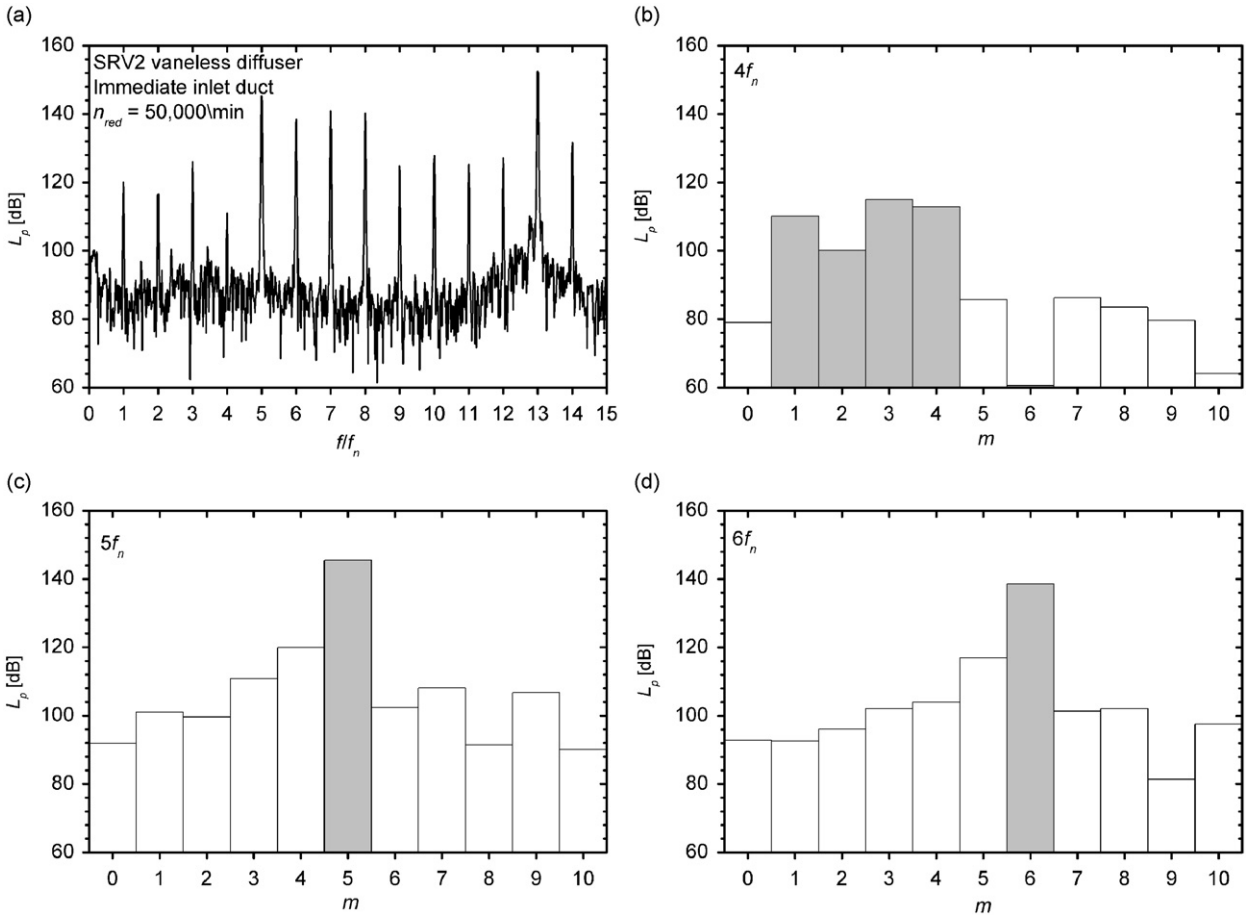

Fig. 14. Sound pressure spectrum and azimuthal mode spectra of the 4–6th rotor-speed harmonic; SRV2; vaneless diffuser; design point; $n_{red} = 50{,}000/\text{min}$; $\dot{m}_{red} = 2.56\,\text{kg/s}$, $\Pi_{tot} = 5.44$: (a) Phase averaged sound pressure spectrum in the immediate inlet duct, (b) azimuthal mode spectrum at $4f_n$, (c) azimuthal mode spectrum at $5f_n$ and (d) azimuthal mode spectrum at $6f_n$.

The mode spectra for the harmonics $i = 5$ and 6 are dominated by the mode order $m = i$. This is not true for the engine order $i = 4$ which, however, is cut off at $4f_n$ and therefore much lower in level than the others in the spectrum (Fig. 14a).

3.3.4. Tip clearance noise

In this section, the spectral components provisionally termed "TCN" (compare Section 3.1) will be investigated.

Kameier [13] and Kameier and Neise [14] studied the aeroacoustic generation mechanism of the TCN in axial turbomachines. In addition to the higher broadband levels reported in the previous published literature, significant sound pressure level increases occurred within limited, almost narrow frequency bands in a region below the BPF component when the tip clearance was enlarged. This TCN component which is a particularly effective noise source was observed when the tip clearance ratio is relatively large and if there is a high enough pressure difference between suction and pressure side of the impeller blades, i.e., at flow rates equal to or smaller than the design flow rate.

Measurements of the pressure fluctuations on the casing wall close to the impeller and on the rotating blades showed that TCN is found in the acoustic far field only if the rotating blade flow instability components are present simultaneously in the near field. This phenomenon is more pronounced at the blade tip than at the hub. The analysis of the pressure spectra measured on the impeller blades and on the casing wall close to the

impeller indicated that the RI components can be interpreted as a fluctuating source or vortex mechanism which rotates relative to the cascade at about half the impeller speed. The circumferential distribution of this rotating source is not uniform and can be represented by a superposition of spatial Fourier components, similar to the higher-order azimuthal modes of sound propagation in circular ducts.

The generation of TCN is explained by the interaction of the RI component with the impeller blades. Neise and Kameier [14] applied Holste's [22,23] model of the interaction of two rotors of different blade numbers and rotor speeds to describe the interaction of an axial fan rotor (subscript "R") with the "RI" and obtained the following relationships for the angular frequency $\omega_{R\&RI}$ and the azimuthal mode order $m_{R\&RI}$ of the resultant interaction noise component:

$$\omega_{R\&RI} = \omega_{TCN} = h\underbrace{Z\Omega_R}_{\omega_{BPF}} - h_\alpha \underbrace{\alpha_{RI}\Omega_{RI}}_{\omega_{RI}}, \tag{5}$$

$$m_{R\&RI} = m_{TCN} = hZ - h_\alpha \alpha_{RI}, \tag{6}$$

where Ω_R and Ω_{RI} are the rotational speeds of the rotor and the RI, respectively. $h = 1,2, \ldots$ stand for the BPF and its harmonics, and $h_\alpha = 1,2, \ldots$ are the harmonic orders (Fourier components) of the RI. With $h = h_\alpha = 1$ and after division by 2π one has from Eq. (5):

$$f_{R\&RI} = f_{TCN} = f_{BPF} - f_{RI}. \tag{7}$$

In the following considerations, the TCN model developed by Neise and Kameier [14] will be applied to the present compressor noise investigation.

Fig. 15 shows for the impeller SRV2 with the vaned diffuser spectra of the sound pressure in the immediate inlet duct and the wall pressure at the casing wall at $n_{red} = 36{,}000$/min. As in the axial fan case, there is a broad spectral hump with added spectral peaks in the wall pressure spectra at about half the BPF, which is marked "RI". Each of these peaks represents one Fourier component α_{RI} of the RI. At a slightly lower frequency another hump ("TCN") is visible in the sound pressure spectrum.

The following frequencies can be read from Fig. 15: $f_{BPF} = 7758$ Hz, $f_{RI} = 4150$ Hz. From Eq. (7) follows for the TCN frequency $f_{TCN} = f_{BPF} - f_{RI} = 3608$ Hz which is within the range 3588–3683 Hz where TCN is observed in the immediate inlet duct.

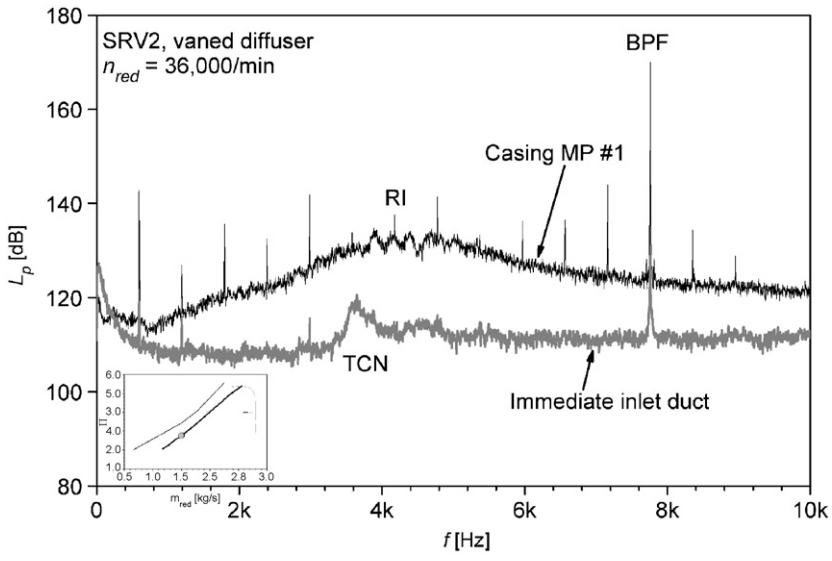

Fig. 15. Spectra of the sound pressure in the immediate inlet duct and the wall pressure at the casing wall (MP#1, compare Fig. 2); SRV2, vaned diffuser, $n_{red} = 36{,}000$/min.

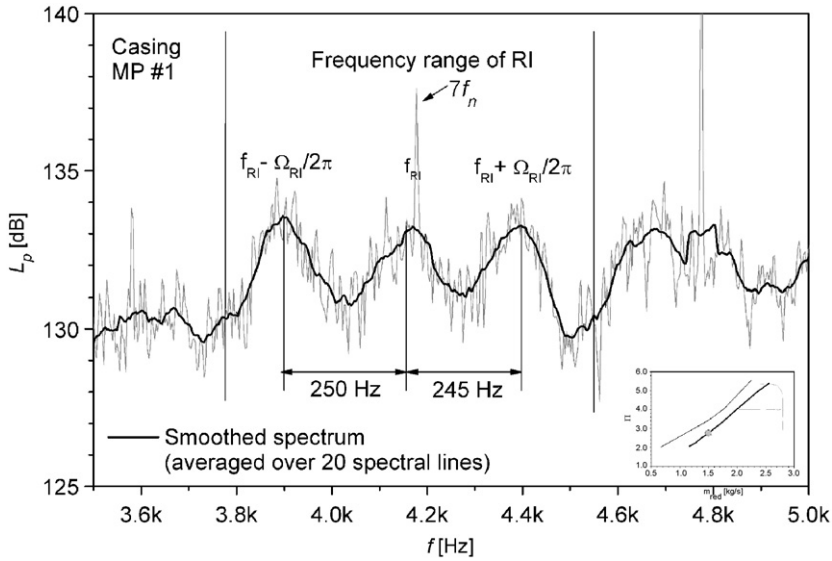

Fig. 16. Wall pressure spectrum at the compressor casing wall (MP#1); SRV2, vaned diffuser, $n_{\mathrm{red}} = 36{,}000/\mathrm{min}$.

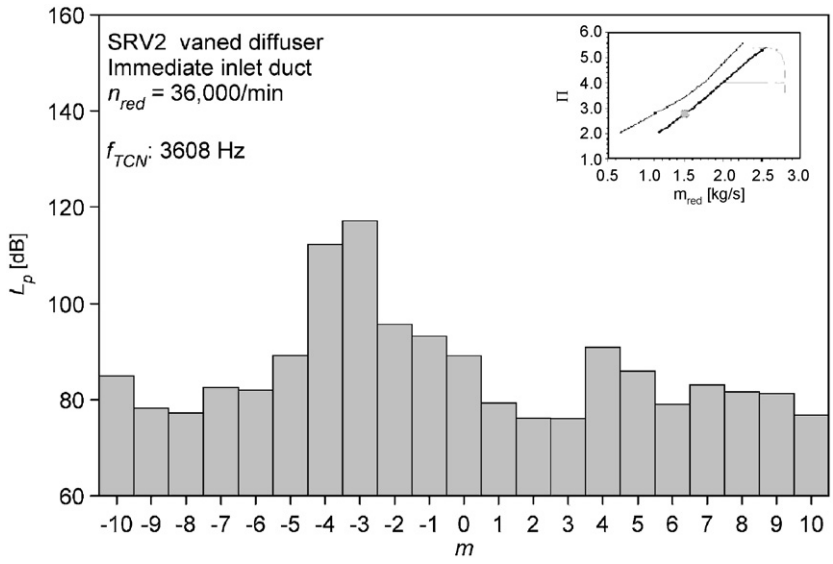

Fig. 17. Azimuthal mode spectrum of tip clearance noise; $f_{\mathrm{TCN}} = 3608\,\mathrm{Hz}$; SRV2; vaned diffuser; $n_{\mathrm{red}} = 36{,}000/\mathrm{min}$.

According to Kameier [13], the frequency difference between two neighbouring peaks is equal to the rotational speed Ω_{RI} of the RI. From Fig. 16, which is an enlarged presentation of the wall pressure spectrum shown in Fig. 15, one finds $\Omega_{\mathrm{RI}} = 245$–$250\,\mathrm{Hz}$.

Combining Eqs. (5) and (6), one obtains for rotational speed Ω_{RI}

$$\Omega_{\mathrm{RI}} = \frac{hZ\Omega_R - \omega_{\mathrm{TCN}}}{hZ - m_{\mathrm{TCN}}} \tag{8}$$

in which all quantities are known except for the azimuthal mode order m_{TCN} of TCN which can be read from the azimuthal mode spectrum of this component in Fig. 17 at $f_{\mathrm{TCN}} = 3608\,\mathrm{Hz}$ where the dominant mode order

is $m_{TCN} = -3$. Inserting all known quantities into Eq. (8) yields $\Omega_{RI}/2\pi = 259.4\,\text{Hz}$ which is very close to the frequency differences between neighboring peaks observed in Fig. 16.

In summary, it is noted that the experimental data measured on the centrifugal compressor are consistent with the TCN model developed by Kameier and Neise [14]. Conversely, one can conclude that the spectral components observed below the BPF in the radial compressor noise spectra in the lower speed range are in fact caused by the secondary flow through the gap between blade tips and the casing.

4. Conclusions

An experimental study of radial compressor noise is described to identify the main noise generation mechanisms for this type of turbomachine. Knowledge of the generation mechanisms is a prerequisite for future low noise compressor design.

Detailed acoustic measurements are carried out on two shroudless radial impeller types "SRV2" and "SRV4" running on a typical compressor test bed. Inlet and outlet blade tip diameters are 157 and 224 mm. Both impellers have 13 main and 13 splitter blades. A vaneless and a vaned outlet diffuser are available for the experiments. The aerodynamics of these compressor stages have been studied extensively, both numerically and experimentally, in previous national research projects.

Sound power measurements at various operating lines of the compressor are made in the anechoically terminated inlet duct following a standardized measurement procedure. Unsteady wall pressure measurements along the radial extent of the compressor casing provide insight into the flow processes within the rotating rotor blade channels.

Acoustic mode measurements are made in the inlet duct at two different axial positions with different diameters: immediately upstream of the compressor intake and 2.1 m farther upstream using rotatable duct sections. Both are equipped with four axial rings with four wall-flush mounted condenser microphones each. The microphones are traversed circumferentially to resolve the spatial sound pressure distribution into azimuthal duct modes of various tonal and narrow-band components. The modal structure of the sound radiated from the compressor impeller reveals the dominant generation mechanisms depending on the tip speed Mach number at the compressor inlet:

- The dominating source mechanisms for the compressor inlet side are
  - TCN at lower impeller tip speed Mach numbers ($Ma_1 < 0.95$).
  - Rotor-alone noise at the BPF and its harmonics at sonic tip speed Mach numbers ($Ma_1 \approx 1$).
  - Rotor-alone noise at the BPF and its harmonics plus buzz-saw noise caused by the shock waves attached to the rotor blades at high rotor speeds.
  - Rotor–stator interaction noise is negligible on the compressor inlet side.
- The dominating source mechanisms for the compressor outlet side are
  - At lower impeller tip speed Mach numbers ($Ma_1 < 0.95$), TCN in case of the compressor with vaneless diffuser, and rotor–stator-interaction noise in case of the vaned diffuser TCN.
  - At high rotor tip speed Mach numbers ($Ma_1 > 1$), blade tone noise due to rotor-alone noise and rotor–stator interaction noise.

The paper represents the first systematic experimental investigation of the tonal and narrow-band spectral components that dominate the noise of centrifugal compressors.

Acknowledgements

The authors gratefully acknowledge the financial support provided by the German Ministry of Economics and Labour via the Arbeitsgemeinschaft industrieller Forschungsgemeinschaften (AiF-Nr. 130941 N) and the Forschungsvereinigung Verbrennungskraftmaschinen (FVV-Nr. 861).

References

[1] H.-J. Feld, S. Aschenbrenner, R. Girsberger, Investigation of acoustic phenomena at the inlet and the outlet of a centrifugal compressor for pressure ratio 4.5, *Proceedings of the ASME TURBO EXPO 2001*, New Orleans, LA, USA, Paper No. 2001-GT-0314.

[2] T. Raitor, W. Neise, H.B. Weyer, Schallentstehung bei Radialverdichtern, Zwischenbericht über das Vorhaben Nr. 781 (AIF-Nr. 13041 N), *Informationstagung Turbinen, FVV-Frühjahrstagung 2003, 3*. April 2003, Frankfurt/Main, Heft R520, S. 129–141.

[3] T. Raitor, W. Neise, R. Mönig, Schallentstehung bei Radialverdichtern, Abschlussbericht über das Vorhaben Nr. 781 (AIF-Nr. 13041 N), *Forschungsvereinigung Verbrennungskraftmaschinen*, Heft 787, Frankfurt/Main, 2004.

[4] T. Raitor, W. Neise, R. Mönig, Schallentstehung bei Radialverdichtern, Abschlussbericht über das Vorhaben Nr. 781 (AIF-Nr. 13041 N), *Informationstagung Turbinen, FVV-Herbsttagung, Pforzheim, 23.9.2004, Forschungsvereinigung Verbrennungskraftmaschinen, Frankfurt/Main*, Heft R527, pp. 125–160.

[5] T. Raitor, W. Neise, R. Mönig, Schallreduzierung bei Radialverdichtern, Abschlussbericht über das Vorhaben FVV-Nr. 861-Informationstagung Turbinen, FVV-Frühjahrstagung 2006, Frankfurt/Main, 30.3.2006, *Forschungsvereinigung Verbrennungskraftmaschinen*, Frankfurt/Main, Heft R534, pp. 195–229.

[6] H. Pak, Radialverdichter hoher Schluckfähigkeit, Abschlussbericht über das Vorhaben Nr. 493, FVV, Frankfurt am Main, 1994.

[7] H. Pak, H. Krain, B. Hoffmann, Flow field analysis of a high pressure ratio centrifugal compressor, AGARD-CP-537, 1993.

[8] H. Krain, B. Hoffmann, H. Pak, Aerodynamics of a centrifugal compressor impeller with transonic inlet conditions, ASME-Paper 95-GT-79, American Society of Mechanical Engineers, New York, 1995.

[9] H. Krain, Radialverdichter hoher Schluckfähigkeit, Abschlussbericht Forschungsvereinigung Verbrennungskraftmaschinen, Frankfurt/Main, Heft 634, 1996.

[10] G. Eisenlohr, P. Dalbert, H. Krain, H. Pröll, F.A. Richter, K.H. Rohne, Analysis of the transsonic flow at the inlet of a high pressure ratio centrifugal impeller, ASME Paper 98-GT-24, American Society of Mechanical Engineers, Conference Stockholm, Sweden, June 1998, p. 11.

[11] H. Krain, B. Hoffmann, Flow physics in high pressure ratio centrifugal compressors, ASME-Paper FEDSM98-4583, Summer Meeting of the American Society of Mechanical Engineers, June 21–25, Washington, DC, USA, 1998, p. 9.

[12] ISO 5136, Acoustics—Determination of Sound Power Radiated into a Duct by Fans and Other Air-Moving Devices—In-duct Method (Revision of ISO 5136:1990) International Standard, International Standards Organization, Geneva, 2003.

[13] F. Kameier, Experimentelle Untersuchung zur Entstehung und Minderung des Blattspitzen-Wirbellärms axialer Strömungsmaschinen, *Fortschritt Berichte VDI Reihe 7*, Nr. 243, VDI Verlag GmbH, Düsseldorf, 1994.

[14] F. Kameier, W. Neise, Rotating blade flow instability as a source of noise in axial turbomachines, *Journal of Sound and Vibration* 203 (1997) 833–853.

[15] J. März, C. Hah, W. Neise, An experimental and numerical investigation into the mechanisms rotating instability, *Journal of Turbomachinery—Transactions of the ASME* 124 (2002) 367–375.

[16] A. McAlpine, M.J. Fisher, B.J. Tester, "Buzz-saw" noise: a comparison of measurement with prediction, *Journal of Sound and Vibration* 290 (2006) 1202–1233.

[17] J.M. Tyler, T.G. Sofrin, Axial flow compressor noise studies, *Transactions of the Society of Automotive Engineers* 70 (1962) 309–332.

[18] C.L. Morfey, M.J. Fisher, Shock-wave radiation from a supersonic ducted rotor, *The Aeronautical Journal of the Royal Aeronautical Society* 74 (1970) 579–585.

[19] D. Hawkings, Multiple pure tone generation by transonic compressors, *Journal of Sound and Vibration* 17 (1971) 241–250.

[20] B.S. Stratford, D.R. Newby, A new look at the generation of buzzsaw noise, AIAA-Paper 77-1343, 1977.

[21] M.J. Fisher, B.J. Tester, P.J.G. Schwaller, Supersonic fan tone noise prediction, in: *AIAA/CEAS Aeroacoustics Conference, 4th* (19th AIAA Aeroacoustics Conference), Toulouse, France, June 2–4, 1998, Collection of Technical Papers—part 1 (A98-30801 07-71).

[22] F. Holste, Ermittlung der aerodynamischen Lärmquellen und Berechnung des abgestrahlten Schallfeldes mittels der im Nahfeld gemessenen Druckschwankungen am Beispiel eines Triebwerksmodells, *VDI-Fortschrittberichte, Reihe 7: Strömungsmechanik, Nr. 272 (1995)*, VDI-Verlag GmbH Düsseldorf 1995 (Dissertation TU Berlin 1995).

[23] F. Holste, W. Neise, Noise source identification in a propfan model by means of acoustical near field measurements, *Journal of Sound and Vibration* 203 (1997) 641–665.